Nonlinear Dyn
https://doi.org/10.1007/s11071-018-4083-7

ORIGINAL PAPER

Nonuniform reinjection probability density function in type V intermittency

Sergio Elaskar · **Ezequiel del Río** · **L. Gutierrez Marcantoni**

Received: 8 September 2017 / Accepted: 13 January 2018

Abstract In this paper, type V intermittency is studied using the M function methodology developed in the last years. This methodology is applied on two different maps to evaluate the reinjection probability density function (RPD), the probability density of laminar lengths and the characteristic relation. We have found that the RPD can be written as an exponential function, where the uniform reinjection is only a singular case. Also, the probability density of laminar lengths can be a nondifferentiable function when the local map has a nondifferentiable point inside the laminar interval. On the other hand, the characteristic relation is not unique, and it depends on the local map. Therefore, the behavior of the reinjection processes and the statistical properties for type V intermittency is wider than the previous studies have described. Finally, it is noted that the M function methodology is a suitable tool to analyze type V intermittency.

Keywords Type V intermittency · M function · RPD · Characteristic relation

1 Introduction

Chaotic intermittency is a route to deterministic chaos, where dynamical systems show transitions between regular phases and chaotic bursts. The regular or laminar phases can be regions of pseudo-equilibrium and/or pseudo-periodic solutions, while at the bursts ones the evolution is chaotic [1–4]. Intermittency was classified in three types called I, II and III, in accordance with the Floquet multipliers of the system or to the eigenvalues in the local Poincaré map [5,6]. Later studies have included other types of chaotic intermittencies: type V, X, on–off (in–out), eyelet and ring [7–13]. Distinct physical phenomena have shown chaotic intermittency [14–22]. Additionally, it has been observed in economical and medical systems [23–25]. We note that a deeper understanding about chaotic intermittency can improve the knowledge of these phenomena.

The local map and the reinjection mechanism determine the chaotic intermittency for one-dimensional maps [1,2,4]. The local map specifies the intermittency type (I, II or III), and the reinjection mechanism returns the system trajectories from the chaotic zone to the laminar one. The reinjection probability density (RPD) function represents this mechanism. The RPD establishes the probability that trajectories are reinjected inside the regular zone. Therefore, to calculate accu-

S. Elaskar (✉) · L. Gutierrez Marcantoni
Departamento de Aeronáutica, FCEFyN, Instituto de Estudios Avanzados en Ingeniería y Tecnología, CONICET and Universidad Nacional de Córdoba, Córdoba, Argentina
e-mail: sergio.elaskar@gmail.com; selaskar@unc.edu.ar

E. del Río
Departamento de Física Aplicada, ETSIAE, Universidad Politécnica de Madrid, Madrid, Spain
e-mail: ezequiel.delrio@upm.es

Published online: 02 February 2018

rately the chaotic intermittency phenomenon, the correct determination of the RPD function is significant. It is important to note there was not a general methodology to calculate the RPD. Then, different approaches were implemented, where the most common one have been to consider an uniform RPD [1–3,5,6].

In the last years, a more general methodology to evaluate the RPD has been developed, which is called here the M function methodology. This new methodology has shown to work accurately for several maps exhibiting type I, II and III intermittencies [4,26–37]. In this paper, we implement this methodology to describe type V intermittency. We show this methodology works accurately for type V intermittency, and the reinjection processes may include RPD functions other than the uniform one. Also, we show that the characteristic relations can acquire other forms than those previously published.

The rest of the paper is organized as follows. In Sect. 2, we describe the type V intermittency characteristics, the M function methodology and two piecewise maps with type V intermittency. The reinjection probability density, the probability density of the laminar lengths and the characteristic relation are given in Sect. 3. Finally, Sect. 4 presents the analysis and conclusions.

2 Models and methods

In this section, the description of type V intermittency, the M function methodology and the studied maps are introduced.

2.1 Type V intermittency

The concept of type V intermittency was, for the first time, introduced in Refs. [38–40]. However, in this section we closely follow the description made in [4].

Type I, II and III intermittencies are characterized by continuous local map. However, type V intermittency appears in maps with nondifferentiable, even discontinuous, local maps.

Type I intermittency begins when one eigenvalue of the fixed point reaches +1 and a channel between the bisector line and the local map appears (tangent bifurcation). On the other hand, type V intermittency occurs when a nondifferentiable point (NDP) and a fixed point collide also forming a channel between the bisector line and the map. But here, there is not a tangent bifurcation because the local map is nondifferentiable or discontinuous at this point.

For type V intermittency, the local map is composed of two maps with different slopes: one for the left side of the NDP and the other one for the right side. These maps describe a "V" [38,39].

Some maps exhibiting type V intermittency were studied in Refs. [38,39]. One of them can be written as:

$$F(x) = \begin{cases} F_1(x) = (x-a)^2 + b & \text{for } x \geq x_d \\ F_2(x) = A\,\mathrm{rnd}(x) + B & \text{for } x < x_d \end{cases} \tag{1}$$

where x_d is the discontinuous point and $\mathrm{rnd}(x)$ is a random number in [0, 1]. The parameters A and B verify that the reinjection occurs below the intersection between the bisector line ($x_{n+1} = x_n$) and the curve $x_{n+1} = F_1(x)$. a and b adjust the variation of function $F_1(x)$ with the control parameter $\varepsilon = F_1(x_d) - x_d$. The value $F_1(x_d)$ moves toward the bisector line for decreasing ε. x_d is a fixed point for $\varepsilon = 0$ ($F_1(x_d) = x_d$). The slope of $F_1(x)$ at the discontinuity point is $\mathrm{d}F_1(x_d)/\mathrm{d}x = s$, which is considered independent of ε. The variation of a and b with s and ε is:

$$\begin{aligned} a &= \frac{4\varepsilon - s}{2} \\ b &= \varepsilon - \frac{s^2}{4} \end{aligned} \tag{2}$$

With random reinjection in an interval around a point, for $s \neq 0$ and $s \neq 1$ when $\varepsilon \to 0$, the average laminar length $\bar{l}$ results:

$$\bar{l} = \frac{\log(\varepsilon)}{\log(s)} + \beta(s) \tag{3}$$

where $\beta(s)$ does not depend on ε. For $s = 1$:

$$\bar{l} = \frac{a}{\varepsilon} + \beta(s) \tag{4}$$

Finally, for $s = 0$:

$$\bar{l} = a \log\left[-\log(\varepsilon)\right] + \beta(s) \tag{5}$$

In [39,40], other two maps were analyzed. The right side of one map, regarding the NDP, can be written as:

$$x_{n+1} = F_2(x_n) = x_n - a\sin(x_n) - \varepsilon \tag{6}$$

The parameter a verifies: $0 < a < 1$, and the control parameter is $\varepsilon \geq 0$. When $\varepsilon = 0$, type V intermittency appears. The laminar length is:

$$l = \left| \int_x^{x_{\text{out}}} \frac{\mathrm{d}x}{a\sin(x) + \varepsilon} \right| = \frac{|\ln(\varepsilon)|}{a} + \Delta(x) \tag{7}$$

where x is the reinjected point, $x_{\text{out}} = \varepsilon/(1-a)$ is the lower end of the laminar interval and $\Delta(x)$ is:

$$\Delta(x) = \frac{1}{a}\ln\left(\frac{2a(1-a)\sin(x)}{1+\cos(x)}\right) \tag{8}$$

In [39], a random RPD with probability $\phi(x)$ between the entrance at point c and the exit point x_{out} was considered. Accordingly, the average laminar length results:

$$\bar{l} = \int_{x_{\text{out}}}^{c} \Delta(x)\phi(x)\mathrm{d}x + \frac{1}{a}|\ln(\varepsilon)| \tag{9}$$

The right part of the second map studied in [39,40] was:

$$x_{n+1} = F_2(x_n) = \zeta x_n - \delta x_n^2 - \varepsilon \tag{10}$$

This map is a generalization of Eq. (1). Following a similar procedure, the average laminar length is:

$$\bar{l} = \frac{|\ln(\varepsilon)|}{1-\zeta} + \int_0^c \frac{1}{1-\zeta}\ln\left(\frac{(1-\zeta)^2\zeta x}{|x\delta + \zeta - 1|}\right)\phi(x)\mathrm{d}x \tag{11}$$

Equations (3), (9) and (11) show that the characteristic relation for type V can be written: $\bar{l} \propto \ln(\varepsilon)$.

Type V intermittency has been observed in real systems. Intermittent chaotic bursting in Hindmarsh–Rose (HR) model had been identified to display type V intermittency characteristics in a nonsmooth map. Near of the period-3 bursting, the intermittent chaotic behavior showed the alternation between phases close to the period-3 bursting and irregular bursting. The scale law of bursting was similar to those of type V intermittent chaos generated in a nonsmooth map [41]. In [42,43], a exhaustive research of the intermittent chaotic bursting and spiking from theoretical models and biological experiments was carried out, and the difference between chaotic spiking and intermittent chaotic bursting was studied. The authors investigated and compared the intermittent chaotic spiking with smooth characteristics and the intermittent chaotic bursting with nonsmooth-like characteristics. The scale law of the averaged length of periodic phase (characteristic relation) for intermittent chaotic bursting was similar to those of type V intermittency generated in nonsmooth systems and type I intermittency simulated in smooth system, while the intermittent chaotic spiking was only classified as type I.

2.2 Evaluation of the RPD function: the M function methodology

The description of the theoretical framework that accounts for a wide class of maps and dynamical systems exhibiting intermittency, called M function methodology, is briefly presented.

Let us to take account of a general one-dimensional map: $x_{n+1} = F(x_n)$. The RPD function, denoted here by $\phi(x)$, determines the probability that trajectories are reinjected into a point x inside the laminar interval. Then, the RPD establishes the statistical behavior of the reinjection trajectories, which depends on the specific form of $F(x)$ [1,2,4].

In this methodology, developed to deal with intermittency, the RPD function is not directly obtained from the numerical or experimental data. A new function, $M(x)$, is previously calculated [4,26–31]:

$$M(x) = \begin{cases} \dfrac{\int_{\hat{x}}^{x} \tau\phi(\tau)\,\mathrm{d}\tau}{\int_{\hat{x}}^{x} \phi(\tau)\,\mathrm{d}\tau}, & \text{if } \int_{\hat{x}}^{x} \phi(\tau)\,\mathrm{d}\tau \neq 0, \\ 0, & \text{otherwise,} \end{cases} \tag{12}$$

where τ represents the reinjected points around the unstable fixed point and $\hat{x}$ is the lower boundary of reinjection point (LBR).

$M(x)$ is an auxiliary function used to evaluate the RPD, and it is a quotient between two integrals which softens the fluctuations of the experimental or numerical data used to construct it [26–33]. On the other hand, $M(x)$ corresponds to the average over the reinjection points in the interval $[\hat{x}, x]$; hence, its numerical estimation is more robust than the direct eval-

uation of the function $\phi(x)$. In addition, the calculation of $M(x)$ from the data series is very simple: $M(x) \cong \frac{1}{N}\sum_{j=1}^{N} x_j$, where the data set (reinjection points) $\{x_j\}_{j=1}^{N}$ must be sorted from the lowest to the highest, i.e., $x_j \leq x_{j+1}$.

In previous papers, we found that $M(x)$ satisfies a linear approximation for a wide class of maps exhibiting type I, II and III intermittencies [26–29,31]:

$$M(x) = \begin{cases} m\left(x - \hat{x}\right) + \hat{x}, & \text{if } \hat{x} \leq x \leq c, \\ 0, & \text{otherwise,} \end{cases} \tag{13}$$

where the slope $m \in (0, 1)$ is a free parameter—determined by the nonlinear map—that governs the reinjection process. Introducing Eq. (13) in Eq. (12), the corresponding RPD function results [26,27,29]:

$$\phi(x) = b(\alpha)\left(x - \hat{x}\right)^{\alpha}, \quad \text{with } \alpha = \frac{2m-1}{1-m}, \tag{14}$$

where $b(\alpha)$ is a normalization parameter, $b(\alpha) = (\alpha+1)/(c-\hat{x})^{\alpha+1}$. The usually considered uniform RPD is recovered for $m = 1/2$ ($\alpha = 0$), i.e., uniform reinjection is obtained as a particular case of the new theoretical formulation. Note that $\phi(x)$ can depart from a uniform reinjection, e.g., $\lim_{x\to 0}\phi(x)$ tends toward infinity when $0 < m < 1/2$ ($\alpha < 0$) and zero, when $1/2 < m < 1$ ($\alpha > 0$).

The $M(x)$ function is determined by the parameters m and $\hat{x}$; also it is easier to obtain than the complete RPD function. Note that M satisfies $M(\hat{x}) = \hat{x}$; then, it allows to evaluate the LBR. As the slope m determines the value of the exponent α in the RPD function (see Eq. 14), it rules the reinjection mechanism and has direct influence on the probability density of the laminar length, on the average laminar length and on the characteristic relation.

For intermittency without noise, the $M(x)$ function is determined by the nonlinear map; each map produces a different $M(x)$ function, defined by the parameters m and $\hat{x}$. Then, the $M(x)$ function stores the nonlinear information of the map [4,35,36].

2.3 Piecewise maps

Maps defined on intervals of the real line have interest in nonlinear dynamics and chaos [44]. In this paper, we study piecewise maps, $F(x)$:

$$F(x) = \begin{cases} f_1(x), & y_0 \leq x < y_1, \\ f_2(x), & y_1 \leq x < y_2, \\ \cdot & \\ \cdot & \\ \cdot & \\ f_m(x), & y_{m-1} \leq x \leq y_m, \end{cases} \tag{15}$$

where $y_1, y_2, \ldots, y_m$ are real numbers.

To analyze the behavior of the M function methodology in type V intermittency, two piecewise one-dimensional maps with type V intermittency are studied (called here Map1 and Map2). It must be noted that the Map2 is a generalization of the map introduced in [39,40].

2.3.1 Map1

The Map1 is built with three functions: linear, quadratic and reinjection. We have selected this map because it is defined by simple functions, but, at the same time, it shows interesting reinjection processes. The map can be written as:

$$F(x) = \begin{cases} F_1(x) = a_1 x + \varepsilon, & \tilde{x} \leq x < 0, \\ F_2(x) = \varepsilon + x + a_2 x^2, & 0 \leq x < x_m, \\ F_3(x) = \tilde{x} + \frac{(y_m - \tilde{x})(y_m - x)^{\gamma}}{(y_m - x_m)^{\gamma}}, & x_m \leq x \leq y_m, \end{cases} \tag{16}$$

where $y_m = F(x_m) = 1$, $\tilde{x}$ is the lower boundary of return [4], $0 < a_1 < 1$ is the slope of the straight line, a_2 is the coefficient of the quadratic term in $F_2(x)$ and finally ε is the control parameter. If $\tilde{x} = 0$, the map is defined inside the interval [0, 1]. Note that $F_1(x)$ is a straight line and $F_2(x)$ is the local map for type I intermittency. The function $F_3(x)$ produces the reinjection process, and it depends on γ. Therefore, this map allows us to analyze different types of reinjection mechanisms using different values of γ. Figure 1 shows this map and one reinjection trajectory.

Map (16) has three fixed points:

$$\begin{aligned} x_1 &= \tfrac{\varepsilon}{1-a_1}, \\ x_2 &= \left(\tfrac{-\varepsilon}{a_2}\right)^{0.5}, \\ x_3 &= \tilde{x} + \tfrac{(y_m - \tilde{x})(y_m - x_3)^{\gamma}}{(y_m - x_m)^{\gamma}}, \end{aligned} \tag{17}$$

If $\varepsilon < 0$, the fixed points x_1 and x_2 exist, and x_1 is less than zero. They are equal zero if $\varepsilon = 0$, and they

disappear for $\varepsilon > 0$. Accordingly, for $\varepsilon = 0$, the fixed points x_1 and x_2 collide in one fixed point $x_0 = 0$.

Also map (16) possesses a discontinuous point at $x = 0$, which collides with the fixed point x_0 for $\varepsilon = 0$. The fixed point vanishes, and type V intermittency can appear for $0 < \varepsilon \ll 1$. The iteration procedure—governed by a_1, a_2 and ε—gives increasing values of x_n generated from an initial one, close to $F(\tilde{x})$. A chaotic burst—govern by $F_2(x)$ and $F_3(x)$—occurs when $x > 0$, which ends when the trajectory is reinjected into a point in the laminar zone. Then, a new iterative process—governed by ε, a_1 and a_2—will be developed producing larger values of the new successive iterative points.

This map can generate two reinjection mechanisms. The first one from points $x < x_0 - c$, where $F_1(x)$ returns the iterative process inside the laminar interval. The second mechanism is from $x > x_0 + c$, where $F_3(x)$ maps points inside the laminar interval as it is indicated in Fig. 1. $x_0 - c$ and $x_0 + c$ are the lower and upper ends of the laminar interval, respectively. Note that $2c$ is the length of the laminar interval.

In this paper, only the second mechanism is considered. It must be noted that the first mechanism produces discontinuous RPD—this phenomenon will be studied in a following paper.

Therefore, the reinjection mechanism is given by $F_3(x)$; then γ drives it, whereas a_1, a_2 and ε determine the laminar phase duration.

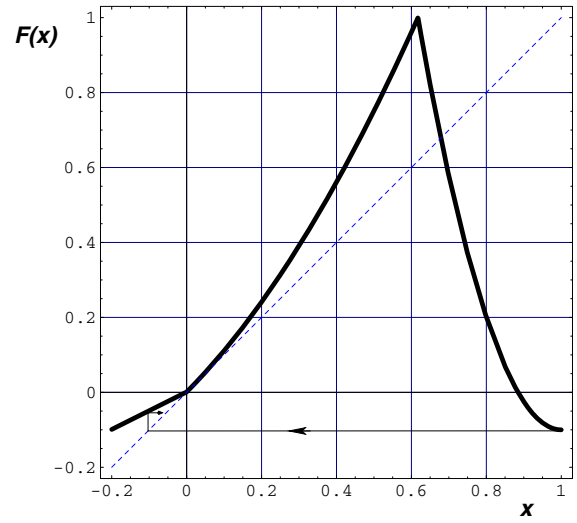

Fig. 1 Map1 for $\gamma = 2$, $\varepsilon = 0.001$, $a_1 = 0.5$, $a_2 = 1$

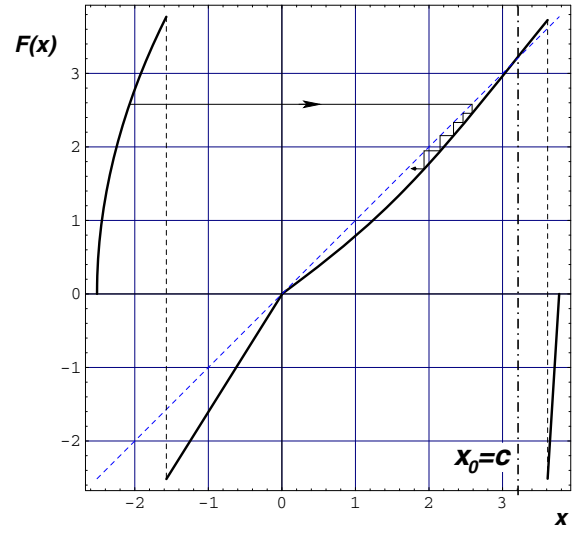

Fig. 2 Map2 for $\gamma = 0.5$, $\varepsilon = 0.001$, $a = 0.25$. The upper end of the laminar interval, $x_0 = c$, is indicated by the vertical dashed-dot line

2.3.2 Map2

The Map2 is given by Eqs. (18) and (19). When $\gamma = 1$ system (18) reduces to those presented in a seminal paper about type V intermittency [40]. This map is shown in Fig. 2.

$$F(x) = \begin{cases} F_1(x) = \left[\frac{f^{1/\gamma}(b_0) - f^{1/\gamma}(b_1)}{b_0 - b_1}(x - b_1) + f^{1/\gamma}(b_1)\right]^{\gamma}, & -0.8\pi \le x < -0.5\pi, \\ F_2(x) = \frac{0.8\pi - g + F_3(x_{\text{out}})}{x_{\text{out}} + 0.5\pi}x + \frac{0.5\pi[F_3(x_{\text{out}}) - g] - 0.8\pi x_{\text{out}}}{x_{\text{out}} + 0.5\pi}, & -0.5\pi \le x < x_{\text{out}}, \\ F_3(x) = x - a\sin(x) - \varepsilon, & x_{\text{out}} \le x < \frac{23\pi}{20}, \\ F_4(x) = \frac{20[0.8\pi + F_3(x_{\text{out}})]}{\pi}x - 19.2\pi - 23F_3(x_{\text{out}}), & \frac{23\pi}{20} \le x \le \frac{6\pi}{5}, \end{cases} \tag{18}$$

where $b_0 = -0.8\pi$, $b_1 = -0.5\pi$, $x_{\text{out}} = \varepsilon/(1 - a)$, g is the gap between $F_2(x_{\text{out}})$ and $F_3(x_{\text{out}})$ and the function $f(x)$ is:

$$f(x) = \frac{10[1.2\pi - F_3(x_{\text{out}})]}{3\pi}x + 3.2\pi - \frac{5F_3(x_{\text{out}})}{3} \tag{19}$$

Equations (18) and (19) allow us to obtain several reinjection processes, being the case studied in [40] only one process ($\gamma = 1$).

The Map2, for $\varepsilon \neq 0$, has one fixed point: $x_0 = \pi + \arcsin(\varepsilon/a)$. In [40], the laminar interval is $x_{\text{out}} \leq x \leq x_0 = c$; where $x_{\text{out}} = \varepsilon/(1-a)$. Note that the amplitude of the laminar interval is as large as the turbulent regime amplitude. However, to compare the new results with the previous ones given in [40], we use the same laminar interval (see Fig. 2). Then, $F_1(x)$ returns the trajectories from the chaotic interval to the laminar one.

3 Results

In this section, the intermittency behavior for Map1 and Map2 is analyzed. To study the reinjection processes for these maps, we shall carry out several numerical experiments or tests considering different reinjection processes.

3.1 Reinjection process for Map1

The first test considers $\gamma = 1$, $\varepsilon = 0.001$, $a_1 = 0.9$, $a_2 = 1$, $N_j = 30{,}000$, $c = 0.1$ and $\tilde{x} = x_0 - c$ where N_j is the number of reinjected points. Note that the lower boundary of return is the lower limit of the laminar interval; then there is no reinjection from points $x < x_0 - c$. The reinjected points inside the laminar interval, $\Delta = [x_0 - c, x_0 + c]$, are mapped by $F_3(x)$ from points placed inside the interval $\Delta_0(x) = F_3^{-1}[x_0 - c, x_0 + c]$.

The theoretical and numerical $M(x)$ functions are shown in Fig. 3. Red points are the numerical data, and the blue line is the minimum square approximation. The $M(x)$ function is a straight line with slope $m \approx 0.5$ ($\alpha \approx 0.0$). Therefore, by Eq. (14), the theoretical RPD can be written as: $\phi(x) = (2c)^{-1}$. Figure 4 shows the numerical and theoretical RPDs. From the figure, we can observe that the reinjection process produces an uniform RPD; also the numerical and theoretical results have a very good agreement.

Other important function to describe the intermittency is the probability density of the laminar lengths, $\psi(l)$, which is a global property of the map [1,4]. The laminar length, $l(x, c)$, is defined as the number of iterations that a trajectory carries out inside the laminar interval, and the probability density of the laminar lengths determines the probability of finding laminar lengths between l and $l + dl$, and it is given by [1,4]:

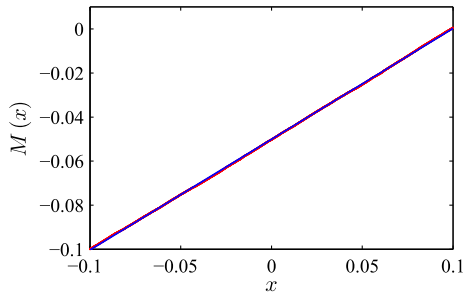

Fig. 3 $M(x)$ function for map (16) with $\gamma = 1$, $\varepsilon = 0.001$, $a_1 = 0.9$, $a_2 = 1$, $N_j = 30{,}000$, $c = 0.1$. Red line is the numerical data, and the solid line represents the theoretical $M(x)$ function. The slope $m \cong 0.5030$ and $\alpha \cong 0.0121$. (Color figure online)

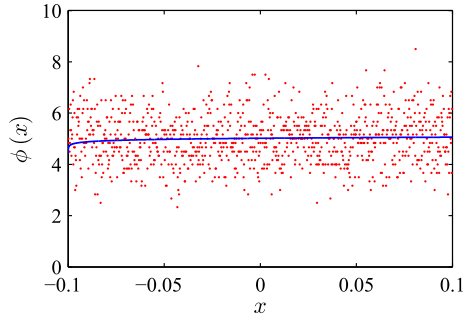

Fig. 4 RPD for map (16) with $\gamma = 1$, $\varepsilon = 0.001$, $a_1 = 0.9$, $a_2 = 1$, $N_j = 30{,}000$, $c = 0.1$. Points are numerical results, and the solid line represents the theoretical RPD

$$\psi(l, c) = \phi[X(l, c)] \left| \frac{\mathrm{d}X(l, c)}{\mathrm{d}l} \right|, \tag{20}$$

where $X(l, c)$ is the inverse of $l(x, c)$. For map (16), $\frac{\mathrm{d}X(l,c)}{\mathrm{d}l}$ is given by:

$$\begin{aligned} \frac{\mathrm{d}X(l,c)}{\mathrm{d}l} &= \varepsilon + x(a_1 - 1), \quad x < 0, \\ \frac{\mathrm{d}X(l,c)}{\mathrm{d}l} &= \varepsilon + a_2 x^2, \quad x \geq 0, \end{aligned} \tag{21}$$

We highlight that $\frac{\mathrm{d}X(l,c)}{\mathrm{d}l}$ is a discontinuous function. From these last equations, we can evaluate $l(x, c)$:

$$\begin{aligned} l(x, c) &= \frac{\ln(\varepsilon) - \ln((a_1 - 1)x + \varepsilon)}{a_1 - 1} + \frac{\arctan\left(c\frac{\sqrt{a_2}}{\sqrt{\varepsilon}}\right)}{\sqrt{a_2\varepsilon}}, \quad x < 0, \\ l(x, c) &= \frac{\arctan\left(c\frac{\sqrt{a_2}}{\sqrt{\varepsilon}}\right) - \arctan\left(x\frac{\sqrt{a_2}}{\sqrt{\varepsilon}}\right)}{\sqrt{a_2\varepsilon}}, \quad x \geq 0, \end{aligned} \tag{22}$$

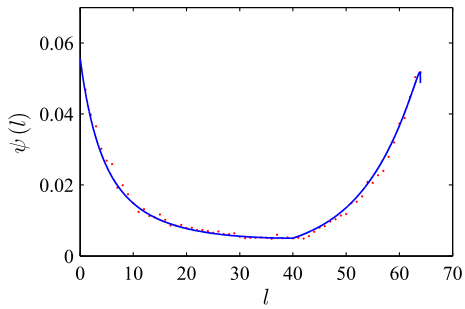

Fig. 5 $\psi(l)$ for map (16) with $\gamma = 1$, $\varepsilon = 0.001$, $a_1 = 0.9$, $a_2 = 1$, $N_j = 30{,}000$, $c = 0.1$. Red points are numerical results, and the blue line represents the theoretical probability density of the laminar lengths. (Color figure online)

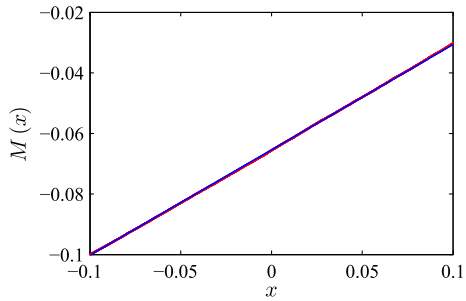

Fig. 6 $M(x)$ function for map (16) with $\gamma = 2$, $\varepsilon = 0.001$, $a_1 = 0.9$, $a_2 = 1$, $N_j = 30{,}000$, $c = 0.1$. Red line is the numerical data, and the solid line represents the theoretical $M(x)$ function. The slope $m \cong 0.348$ and $\alpha \cong -0.466$. (Color figure online)

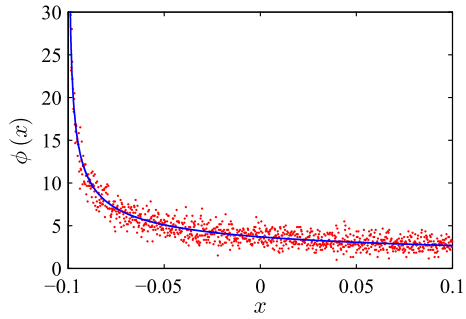

Fig. 7 RPD for map (16) with $\gamma = 2$, $\varepsilon = 0.001$, $a_1 = 0.9$, $a_2 = 1$, $N_j = 30{,}000$, $c = 0.1$. Points are numerical results, and the solid line represents the theoretical RPD

Figure 5 shows the numerical and theoretical probability density of the laminar lengths for the same parameters of Figs. 3 and 4. The theoretical $\psi(l)$ was evaluated using Eq. (20), and it is shown as a blue line, whereas the points are the numerical results. There is a very good accuracy between the theoretical evaluation and the numerical data. The probability density of the laminar lengths has two behaviors: one for $0 < l \leq 40$, in which $\psi(l)$ is a decreasing function and corresponds to points reinjected inside $[x_0, x_0 + c]$; the other one appears for $l > 40$ and it is given by points reinjected in $[x_0 - c, x_0)$.

We study a second test which considers the same parameters used in the previous test, with the exception of the exponent γ, which now is $\gamma = 2$; i.e., $F_3(x)$ becomes a nonlinear function. The $M(x)$ function is shown in Fig. 6. The red and blue lines show the numerical data and minimum square approach, respectively. From this figure, we can note that the $M(x)$ function can be considered as a linear function. From the minimum square approach, we have obtained $m \cong 0.3348$ and $\alpha \approx -0.5$. The theoretical RPD results as (see Eq. 14):

$$\phi(x) \cong 1.118\,(x + 0.1)^{-0.5} \tag{23}$$

Figure 7 shows the numerical and theoretical RPDs. The theoretical RPD is evaluated using the linear approximation for the $M(x)$ function. The red points are the numerical RPD, and the solid blue line represents the theoretical RPD which is very accurate approximation to the numerical data. The RPD is a decreasing function with a high concentration of reinjection trajectories close to lower limit of the laminar interval, $x_0 - c$. Similar results have been documented for other types of intermittency [26,27,30], and there is theoretical studies about it [4,35].

The third numerical case uses the same parameters of the first test, but in this case $\gamma = 0.5$, i.e., $F_3(x)$ is again a nonlinear function, but different those used in Test 2. Figure 8 shows the numerical and theoretical $M(x)$ functions, which result lineal functions with slope $m \cong 0.6639$ ($\alpha \cong 1$). Then the RPD results:

$$\phi(x) \cong 50.0\,(x + 0.1) \tag{24}$$

Note that the RPD is not uniform, and it is an increasing function with high concentration of reinjection points close to the upper end of the laminar interval, $x_0 + c$. The theoretical $\phi(x)$ function increases linearly as x increases (Fig. 9).

Figure 10 shows the numerical and theoretical probabilities density of the laminar lengths. The solid line shows the theoretical results, and it was calculated by

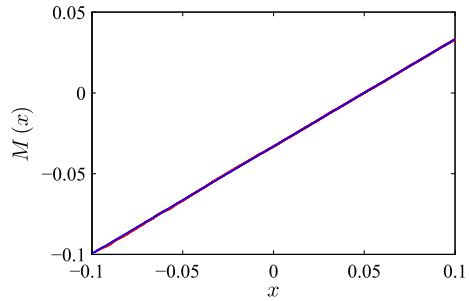

Fig. 8 $M(x)$ function for map (16) with $\gamma = 0.5$, $\varepsilon = 0.001$, $a_1 = 0.9$, $a_2 = 1$, $N_j = 30{,}000$, $c = 0.1$. Red line is the numerical data, and the solid line represents the theoretical $M(x)$ function. The slope $m \cong 0.6639$ and $\alpha \cong 0.975$. (Color figure online)

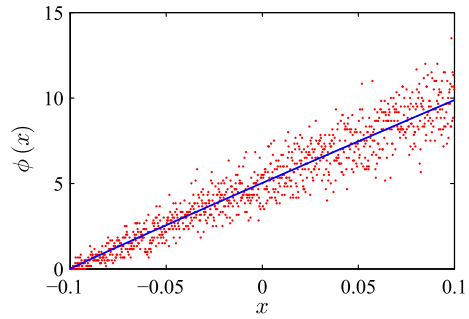

Fig. 9 RPD for map (16) with $\gamma = 0.5$, $\varepsilon = 0.001$, $a_1 = 0.9$, $a_2 = 1$, $N_j = 30{,}000$, $c = 0.1$. Points are numerical results, and the solid line represents the theoretical RPD

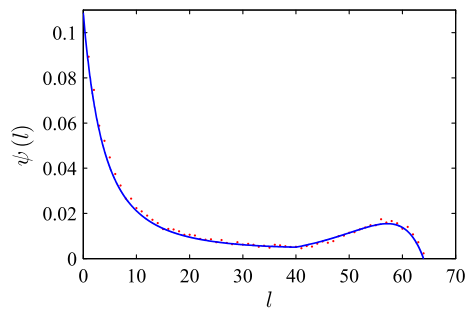

Fig. 10 $\psi(l)$ for map (16) with $\gamma = 0.5$, $\varepsilon = 0.001$, $a_1 = 0.9$, $a_2 = 1$, $N_j = 30{,}000$, $c = 0.1$. Points are numerical results, and the solid line represents the theoretical probability density of the laminar lengths

Eq. (20). Red points represent the numerical data. The theoretical result shows high accuracy regarding the numerical data.

To evaluate the "duration" of the laminar phases, we also consider the average laminar length, which can be evaluated as [1,2,4]:

$$\bar{l} = \int_0^{l_m} \psi(l, c)\, l \, \mathrm{d}l = \int_{-c}^{c} \phi(x)\, l(x, c)\, \mathrm{d}x \tag{25}$$

where l_m is the highest laminar length.

From the numerical data and the theoretical results shown in Figs. 5 and 10, we can evaluate the first integral in (25).

On the other hand, by Eqs. (14), (22) and (25), we can obtain the average laminar length and the characteristic relation:

$$\bar{l} = \int_{-c}^{0} \phi(x) l(x, c)|_{x<0} \mathrm{d}x + \int_{0}^{c} \phi(x) l(x, c)|_{x>0} \mathrm{d}x \tag{26}$$

We have found that for $\gamma = 1$, the exponent $\alpha \cong 0$. For $\alpha = 0$, we can integrate analytically Eq. (25); then, the average laminar length results:

$$\bar{l} = \left(1 - \frac{\varepsilon}{c(a_1-1)}\right) \frac{\ln(\varepsilon)}{2(a_1-1)} + \frac{(\varepsilon-(a_1-1)c)\ln(\varepsilon-(a_1-1)c)}{2c(a_1-1)^2} + \frac{1}{2(a_1-1)} + \frac{\arctan\left(c\frac{\sqrt{a_2}}{\sqrt{\varepsilon}}\right)}{2\sqrt{a_2\varepsilon}} + \frac{\ln\left(1+\frac{a_2c^2}{\varepsilon}\right)}{4a_2c} \tag{27}$$

Figure 11 shows the average laminar length as function of the control parameter ε for $\gamma = 1$—then, it shows the characteristic relation. The blue line represents Eq. (27), and the red points are numerical results. From this figure, the characteristic relation, for $\varepsilon \to 0$, can be approximated as:

$$\bar{l} \propto \varepsilon^{-\beta} \tag{28}$$

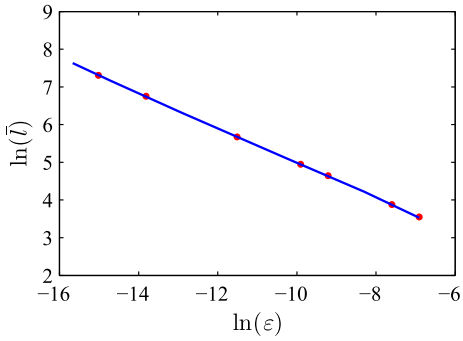

Fig. 11 $\ln(\bar{l})$ as function of $\ln(\varepsilon)$ for map (16) with $\gamma = 1$. Points are numerical data, and the solid line represents the theoretical results, Eq. (27)

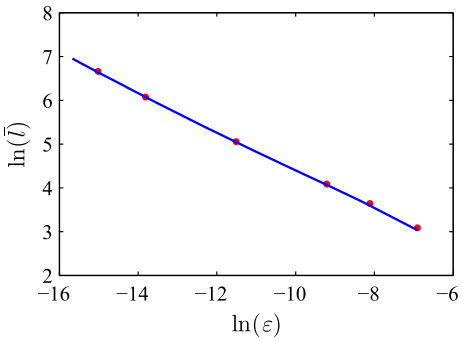

Fig. 12 Variation of $\ln(\bar{l})$ as function of $\ln(\varepsilon)$ for map (16) with $\gamma = 0.5$. Points are numerical results, and the solid line represents the theoretical approximation, Eq. (29)

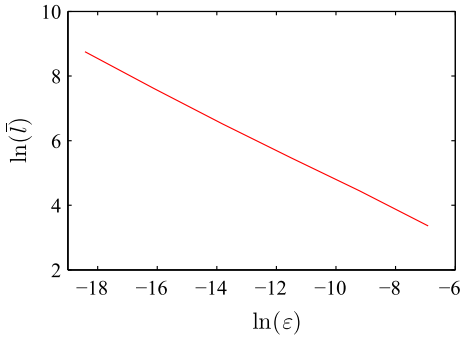

Fig. 13 Numerical variation of $\ln(\bar{l})$ as function of $\ln(\varepsilon)$ for map (16) with $\gamma = 0.75$

Table 1 Values of α, Eq. (14), for different values of ε. $\gamma = 0.75$

ε	α
1×10^{-3}	0.3320
1×10^{-4}	0.3322
1×10^{-5}	0.3232
1×10^{-6}	0.3244
1×10^{-7}	0.3376
1×10^{-8}	0.3332

Table 2 Variation of exponent α for different a_1 and γ

$a_1 - \gamma$	$\gamma = 0.5$	$\gamma = 0.75$	$\gamma = 1$
$a_1 = 0.25$	1.0202	0.3378	0.0145
$a_1 = 0.50$	1.0036	0.3320	0.0113
$a_1 = 0.90$	0.9750	0.3320	0.0121

where $\beta \cong 0.5$.

For $\gamma = 0.5$, we have calculated $\alpha \cong 1$. Then, the RPD can be written as: $\phi(x) = b(x + c)$, and we can obtain the theoretical expression for the average laminar length, which is given by Eq. (29).

$$\bar{l} = \frac{2c^2(a_1-1)^2\sqrt{(a_2\varepsilon)}\left(c\sqrt{a_2/\varepsilon}\right) + a_2\varepsilon\left((a_1-1)c(3c(a_1-1)-2\varepsilon) + 2(\varepsilon-(a_1-1)c)^2\left(\ln(\varepsilon) - \ln\left(\varepsilon-(a_1-1)\right)\right)\right)}{8a_2c^2\varepsilon(a_1-1)^3} + \frac{2c\left(1-\ln(\varepsilon)+\ln(\varepsilon+a_2c^2)\right) - \frac{2\sqrt{\varepsilon}}{\sqrt{a2}}\left(c\sqrt{a_2/\varepsilon}\right)}{8a_2c^2} \tag{29}$$

Figure 12 shows the characteristic relation for $\gamma = 0.5$. The blue line represents Eq. (29), and the red points are numerical evaluations. When $\varepsilon \to 0$, the characteristic relation can be again expressed by Eq. (28) with $\beta \cong 0.5$.

From the previous tests, we have found there are a high accuracy between numerical and theoretical average laminar lengths.

We also carried out several numerical experiments using $\gamma = 0.75$. We have considered $\varepsilon = 1 \times 10^{-3} - 1 \times 10^{-8}$. For all these tests, $\alpha \cong 1/3$ (see Table 1).

Figure 13 shows $\ln(\bar{l})$ as function of $\ln(\varepsilon)$ for $\gamma = 0.75$. The relation can be represented by a straight line with slope ≈ -0.5; then, the characteristic relation can be written as $\bar{l} \propto \varepsilon^{-0.5}$.

To study the sensibility of the reinjection process regarding the slope a_1, we evaluate theoretical and numerically the exponent α for different values of a_1. The theoretical α for different values of a_1 and γ is given in Table 2.

We have found a very good accuracy between them, and we have obtained that a_1 does not influence the reinjection process. The reinjection is mainly ruled by the exponent γ. Therefore, for small c, the local map does not influence the reinjection mechanism.

In previous works, the following relation was analytically found [4,26,35]:

$$\alpha = \frac{1}{\gamma} - 1 \tag{30}$$

It was applied successfully for maps with continuous local maps [4,35]. However, Eq. (30) has also been valid for all the tests here studied. From Table 2, for $\gamma = 1$ we have obtained $\alpha \cong 0$ (see also Figs. 3, 4); for $\gamma = 0.5$, we have calculated $\alpha \cong 1$ (see Figs. 8, 9), and for $\gamma = 0.75$ we have found $\alpha \cong 1/3$. On the other hand, for $\gamma = 2$ we have obtained $\alpha \cong -0.5$ (see Figs. 6, 7).

All previous tests verify $\tilde{x} = x_0 - c$, which does not allow reinjections from points $x < x_0 - c$. However, the RPDs functions show different behaviors depending on the γ value. We have found three different behaviors:

- For $\gamma = 1$. there is uniform reinjection.
- For $\gamma > 1$, the RPD is a decreasing function with a high concentration of reinjection points close to the lower boundary of reinjection.
- For $\gamma < 1$, the RPD is an increasing function with a high concentration of reinjection points close to upper end of the laminar interval.

We highlight that $M(x)$ functions are lineal for all tests, and the M function methodology has captured accurately the numerical results.

On the other hand, we have found that the characteristic relation can be written as: $\bar{l} \propto \varepsilon^{-0.5}$ for different reinjection processes.

3.2 Reinjection process for Map2

For all tests, to obtain the statistical variables of the reinjection processes the M function methodology is applied.

Three different tests are analyzed: $\gamma = 1$, $\gamma = 0.5$ and $\gamma = 1.5$; each one of them produces a different reinjection mechanism.

3.2.1 Test 1

The first test corresponds to those analyzed in [40], then $\gamma = 1$, and the laminar interval is $x_{\text{out}} \leq x \leq x_0$. Figure 14 shows the numerical $M(x)$ function (red), and its minimum square approximation (blue) for $\varepsilon = 0.0001$, $a = 0.25$, $\gamma = 1$, $N_j = 50{,}000$. $M(x)$ can be represented by a linear function with slope $m \cong 0.4845$ ($\alpha \cong -0.06$). Accordingly, the RPD function results:

$$\phi(x) \cong \frac{(x - x_{\text{out}})^{\alpha}}{x_0 - x_{\text{out}}} \cong \frac{1}{x_0 - x_{\text{out}}} \tag{31}$$

Note that Eq. (30) is verified: $\alpha \cong 0$.

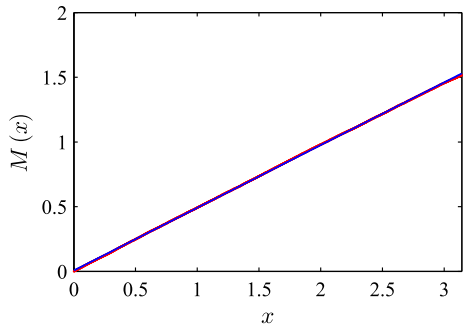

Fig. 14 $M(x)$ functions for Eq. (18). Red: numerical. Blue: minimum square. Parameters: $\varepsilon = 0.0001$, $a = 0.25$, $\gamma = 1$, $N_j = 50{,}000$. (Color figure online)

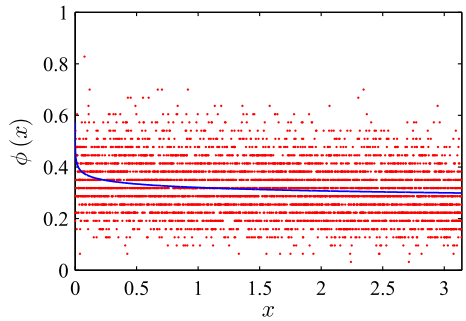

Fig. 15 Theoretical and numerical RPDs functions for Eq. (18). Red: numerical. Blue: theoretical. Parameters: $\varepsilon = 0.0001$, $a = 0.25$, $\gamma = 1$, $N_j = 50{,}000$. (Color figure online)

The comparison between numerical and theoretical RPDs is shown in Fig. 15. The blue line is the theoretical function, which is evaluated using Eq. (31).

Figure 16 shows the comparison between numerical and theoretical probability density of the laminar lengths, $\psi(l, c)$, which is calculated using Eq. (20) where

$$\frac{\mathrm{d}X(l,c)}{\mathrm{d}l} = -(a\sin(x) + \varepsilon) \tag{32}$$

Integrating this equation, we can obtain the relation between the laminar length and the reinjection point (see Eq. 33).

$$l(x, x_{\text{out}}) = \frac{1}{\sqrt{a^2 - \varepsilon^2}} \times \left[\ln \left| \frac{\varepsilon \tan(x/2) + a - \sqrt{a^2 - \varepsilon^2}}{\varepsilon \tan(x/2) + a + \sqrt{a^2 - \varepsilon^2}} \right| - \ln \left| \frac{\varepsilon \tan(x_{\text{out}}/2) + a - \sqrt{a^2 - \varepsilon^2}}{\varepsilon \tan(x_{\text{out}}/2) + a + \sqrt{a^2 - \varepsilon^2}} \right| \right] \tag{33}$$

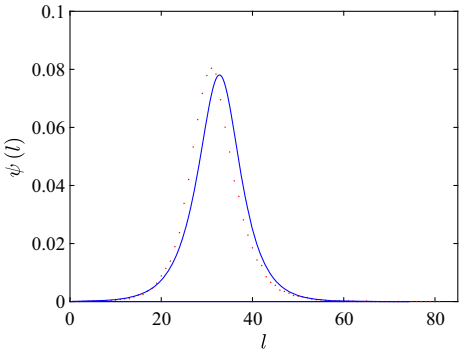

Fig. 16 Theoretical and numerical $\psi(l, c)$ functions for Eq. (18). Red: numerical. Blue: theoretical. Parameters: $\varepsilon = 0.0001$, $a = 0.25$, $\gamma = 1$, $N_j = 50{,}000$. (Color figure online)

The previous results are in agreement with those included in [40]. But, other reinjection processes did not study previously can appear for Map2. Therefore, we will analyze system (18)–(19) for different values of the parameter γ.

3.2.2 Test 2

The second test uses the same parameters of the first test, but $\gamma = 0.5$. Then, the main parameters are: $\varepsilon = 0.0001$, $a = 0.25$, $\gamma = 0.5$, $N_j = 50{,}000$. The laminar interval is $x_{\text{out}} \leq x \leq x_0$. Figure 17 shows the numerical M function (red) and its minimum square approximation (blue). $M(x)$ can be approached by a linear function with slope $m \cong 0.66$ ($\alpha \cong 0.94$). Then, by Eq. (14), the RPD is:

$$\phi(x) \cong \frac{1.94(x - x_{\text{out}})^{0.94}}{(x_0 - x_{\text{out}})^{1.94}} \tag{34}$$

Theoretical and numerical RPDs are displayed in Fig. 18. The theoretical prediction, Eq. (30), establishes $\alpha = 1$. Therefore, the error in the evaluation of the α exponent is 6/100, which is low considering the large laminar interval (the laminar iterations can reach the same length that the turbulent ones).

Figure 19 shows the theoretical and numerical probability density of the laminar lengths, $\psi(l, c)$, which is calculated using Eqs. (20) and (33). Red points represent numerical data, and the theoretical result is the blue line. All the figures show a good accuracy between numerical data and theoretical predictions although the large laminar interval.

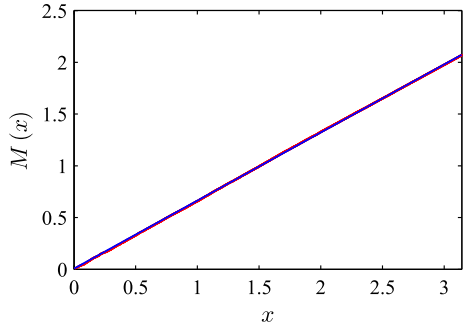

Fig. 17 $M(x)$ functions for Eq. (18). Red: numerical. Blue: minimum square. Parameters: $\varepsilon = 0.0001$, $a = 0.25$, $\gamma = 0.5$, $N_j = 50{,}000$. (Color figure online)

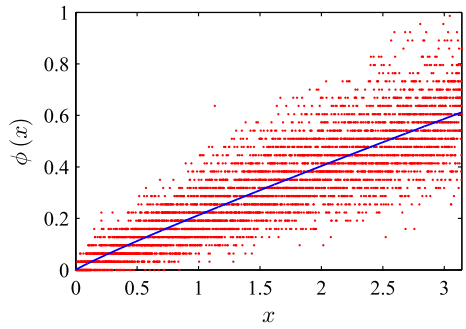

Fig. 18 Theoretical and numerical RPD functions for Eq. (18). Red: numerical. Blue: theoretical. Parameters: $\varepsilon = 0.0001$, $a = 0.25$, $\gamma = 0.5$, $N_j = 50{,}000$. (Color figure online)

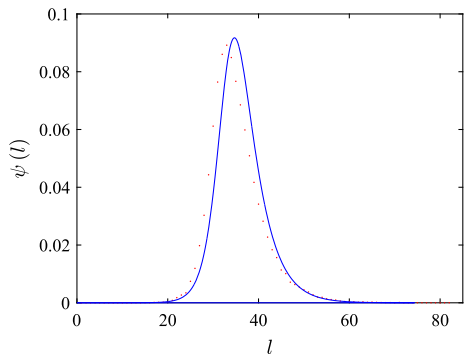

Fig. 19 Theoretical and numerical $\psi(l, c)$ functions for Eq. (18). Red: numerical. Blue: theoretical. Parameters: $\varepsilon = 0.0001$, $a = 0.25$, $\gamma = 0.5$, $N_j = 50{,}000$. (Color figure online)

It must be noted that M function methodology can capture accurately the RPD. In this test, $\phi(x)$ increases with x. There is a high concentration of reinjection points close to the upper end of the laminar interval x_0. Again the M function methodology has been a suitable tool to describe the reinjection process.

3.2.3 Test 3

This test has the same parameters that Test 1, but $\gamma = 1.5$. The laminar interval is $x_{\text{out}} \leq x \leq x_0$. The numerical $M(x)$ function (red) and its minimum square approach are shown in Fig. 20. Note that a straight line is a good approach for $M(x)$ function ($m \cong 0.3878$ and $\alpha \cong -0.3772$).

The RPD is calculated using the M function methodology:

$$\phi(x) \cong \frac{0.6228(x - x_{\text{out}})^{-0.3772}}{(x_0 - x_{\text{out}})^{0.6228}} \tag{35}$$

The results calculated with Eq. (35) are compared with numerical data in Fig. 21. The RPD is again a nonlinear function, which decreases with increasing x. Note the high concentration of reinjected points close to the lower limit of the laminar interval x_{out}.

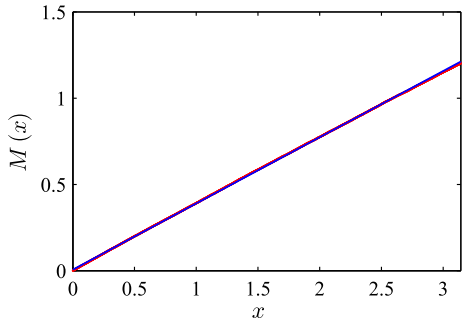

Fig. 20 M functions for Eq. (18). Red: numerical. Blue: minimum square. Parameters: $\varepsilon = 0.0001$, $a = 0.25$, $\gamma = 1.5$, $N_j = 50{,}000$. (Color figure online)

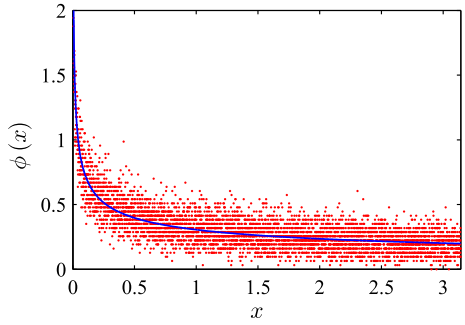

Fig. 21 Theoretical and numerical RPD functions for Eq. (18). Red: numerical. Blue: theoretical. Parameters: $\varepsilon = 0.0001$, $a = 0.25$, $\gamma = 1.5$, $N_j = 50{,}000$. (Color figure online)

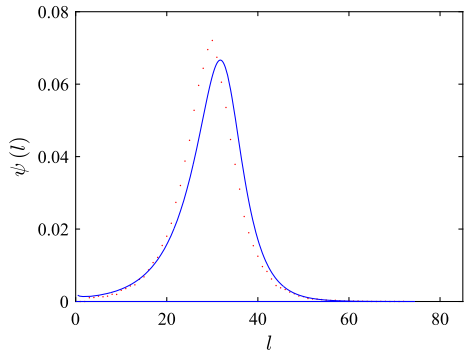

Fig. 22 Theoretical and numerical $\psi(l)$ functions for Eq. (18). Red: numerical. Blue: theoretical. Parameters: $\varepsilon = 0.0001$, $a = 0.25$, $\gamma = 1.5$, $N_j = 50{,}000$. (Color figure online)

Finally, the probability density of the laminar lengths is shown in Fig. 22. The theoretical $\phi(x)$ and $\psi(l)$ have good accuracy with regard the numerical results.

3.2.4 Characteristic relation

Equation (33) establishes the relation between the laminar length, l, and the reinjection point, x. For $\varepsilon \to 0$, this equation can be can be approximated by [40]:

$$l(x, x_{\text{out}}) \cong \frac{|\ln(\varepsilon)| + \ln(2a(1-a)) + \ln[\tan(x/2)]}{a} \tag{36}$$

Therefore, using Eqs. (14) and (36), the average laminar length results:

$$\bar{l} = \int_{x_{\text{out}}}^{x_0} \frac{b(x - x_{\text{out}})^{\alpha} \left[|\ln(\varepsilon)| + \ln\left(2a(1-a)\tan\left(\frac{x}{2}\right)\right)\right]}{a} \mathrm{d}x \tag{37}$$

where $b = (\alpha + 1)\left[(x_0 - x_{\text{out}})^{-\alpha-1}\right]$. Then, the average laminar length can be approximated by:

$$\bar{l} \approx \frac{|\ln(\varepsilon)|}{a} + k \tag{38}$$

where k is a constant. To obtain this equation, we have considered that x_{out} does not depend on ε in the last term of Eq. (37).

Figure 23 shows $\bar{l}$ as function of $\ln(\varepsilon)$ for uniform reinjection ($\gamma = 1$ and $\alpha = 0$). Numerical data are shown as red points and the blue line is evaluated using minimum square, which has a slope $|h_n| \cong 3.4$.

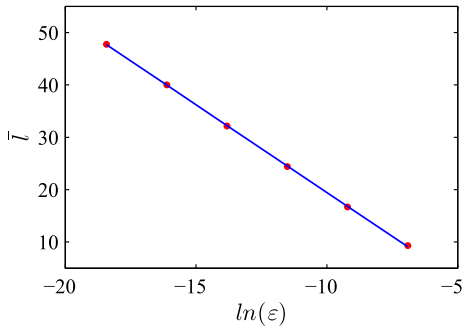

Fig. 23 Characteristic relation for Eq. (18) when $a = 0.25$, $\gamma = 1.0$, $N_j = 50{,}000$, $c = 0.1$. Red: numerical data. Blue: minimum square approach. (Color figure online)

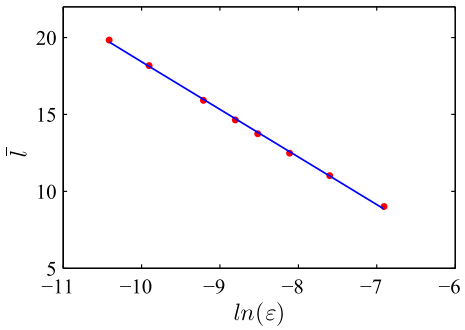

Fig. 24 Characteristic relation for Eq. (18) when $a = 0.25$, $\gamma = 1.5$, $N_j = 30{,}000$, $c = 0.1$. Red: numerical data. Blue: minimum square approach. (Color figure online)

Table 3 Values of α, Eq. (14), for different values of ε. $\gamma = 1.5$

ε	α
1×10^{-3}	-0.3185
5×10^{-4}	-0.3145
3×10^{-4}	-0.323
2×10^{-4}	-0.322
1.5×10^{-4}	-0.32
1×10^{-4}	-0.332
5×10^{-5}	-0.333
3×10^{-5}	-0.343

Remember that Eq. (38) is an approximated equation which predicts a slope $|h| = 1/a = 4$.

To analyze nonuniform reinjection process, we evaluate several tests for $\gamma = 1.5$ and different values of ε. Table 3 shows the exponent α calculated using the M function methodology for $\varepsilon = 1 \times 10^{-3} - 3 \times 10^{-5}$. The theoretical prediction, Eq. (30), is verified ($\alpha \cong -1/3$).

On the other hand, Fig. 24 shows $\bar{l}$ as function of $\ln(\varepsilon)$ for $\gamma = 1.5$ and $\alpha \cong -1/3$. Red points are the numerical data, and the blue line is the minimum square approach. As in the uniform reinjection test, the relation $\bar{l} = \bar{l}(\ln \varepsilon))$ is a straight line, but the numerical slope is smaller, $|h_n| \cong 3.1$. It must be noted that the assumptions used to obtain Eq. (38) introduce errors in the slope evaluation. However, Eq. (38) captures the linear relation between $\bar{l}$ and $\ln(\varepsilon)$ for uniform and nonuniform RPDs.

4 Analysis and conclusions

In this work, we have applied the M function methodology to describe the reinjection process for type V intermittency, which occurs when the local map has a nondifferentiable or discontinuous point. This methodology had worked accurately for type I, II and III intermittencies, where the local map is continuous. Here, we have shown that this methodology also works accurately for type V intermittency. It can capture very well the RPD function, and other intermittency statistical properties (probability density of the laminar lengths and average laminar length), for different maps and different reinjection mechanisms.

We have studied two maps. The local map for the first one, Eq. (16), is composed of two simple functions, one is linear and the other one is quadratic. However, the local part of the second piecewise map, Eqs. (18)–(19), is given by a sine function. Also, the used laminar intervals were very dissimilar for both maps. For map (16), it was small ($c \ll 1$) and symmetrical around the vanished fixed point, but for map (18), the laminar interval only considered positive values and it was large ($c \approx \pi$). But, in spite of these differences the M function methodology produced accurate results.

We have shown that the RPD can be a nonuniform function. It is described by an exponential function with exponent α. To obtain the analytical RPD is only necessary to evaluate the slope m of the $M(x)$ function (α depends on m). The uniform reinjection is only a singular case when $m = 1/2$ ($\alpha = 0$).

Also, we have obtained that the local map does not influence the reinjection process when $c \ll 1$. However, if the local map is nondifferentiable, the laminar

length, $l(x, c)$, and the probability density of the laminar lengths, $\psi(l)$, are nondifferentiable too.

For Map1, the probability density of the laminar lengths, $\psi(l)$, has two behaviors: the first one for reinjected points inside the interval $-c \leq x \leq x_0$, which need more than $\approx$ 40 iterations to leave the laminar interval; the second one for reinjected points in $x_0 < x \leq c$ which need less than $\approx$ 40 iterations to leave the laminar interval. Then, $\psi(l)$ is nondifferentiable function for $l \approx 40$ (see Figs. 5, 10). For Map2, $\psi(l)$ is a differentiable function with a high concentration between $20 < l < 40$ (see Figs. 16, 19, 22). $\psi(l)$ is a differentiable function because the laminar interval only contains points verifying $x > 0$; then, it is not symmetrical around the vanished fixed point.

The average laminar length, $\bar{l}$, acquires different form for each map. The Map1 verifies $\bar{l} \propto \varepsilon^{-\beta}$; however, the characteristic relation for Map2 is $\bar{l} \propto \ln(\varepsilon)$. Therefore, there is not only one characteristic relation for type V intermittency, and it depends on the local map.

Finally, we highlight that the reinjection mechanism for type V intermittency has a wide behavior, and the uniform reinjection is only a particular case. The reinjection depends, mainly, on the global part of the map. Also, it must be highlighted that we have not considered the reinjection process from points adjacent to the laminar interval, which can produce discontinuous RPDs. This phenomenon will be analyzed in a following paper.

Acknowledgements This research was supported by CONICET, Universidad Nacional de Córdoba, Universidad Politécnica de Madrid, and the Spanish Ministry of Science and Innovation (MICINN) under Project No. EPS2013-41078-R.

References

1. Schuster, H., Just, W.: Deterministic Chaos. Wiley VCH, Mörlenbach (2005)
2. Nayfeh, A., Balachandran, B.: Applied Nonlinear Dynamics. Wiley, New York (1995)
3. Marek, M., Schreiber, I.: Chaotic Behaviour of Deterministic Dissipative Systems. Cambridge University Press, Cambridge (1995)
4. Elaskar, S., del Rio, E.: New Advances on Chaotic Intermittency and Its Applications. Springer, New York (2017)
5. Manneville, P., Pomeau, Y.: Intermittency and Lorenz model. Phys. Lett. A **75**, 1–2 (1979)
6. Manneville, P.: Intermittency, self-similarity and $1/f$ spectrum in dissipative dynamical systems. J. Phys. **41**, 1235–1243 (1980)
7. Kaplan, H.: Return to type I intermittency. Phys. Rev. Lett. **68**, 553–557 (1992)
8. Price, T., Mullin, P.: An experimental observation of a new type of intermittency. Physica D **48**, 29–52 (1991)
9. Platt, N., Spiegel, E., Tresser, C.: On–off intermittency: a mechanism for bursting. Phys. Rev. Lett. **70**, 279–282 (1993)
10. Pikovsky, A., Osipov, G., Rosenblum, M., Zaks, M., Kurths, J.: Attractor–repeller collision and eyelet intermittency at the transition to phase synchronization. Phys. Rev. Lett. **79**, 47–50 (1997)
11. Lee, K., Kwak, Y., Lim, T.: Phase jumps near a phase synchronization transition in systems of two coupled chaotic oscillators. Phys. Rev. Lett. **81**, 321–324 (1998)
12. Hramov, A., Koronovskii, A., Kurovskaya, M., Boccaletti, S.: Ring intermittency in coupled chaotic oscillators at the boundary of phase synchronization. Phys. Rev. Lett. **97**, 114101 (2006)
13. Stavrinides, S., Anagnostopoulos, A.: Chapter 9: the route from synchronization to desynchronization of chaotic operating circuits and systems. In: Banerjee, S., Rondoni, L. (eds.) Applications of Chaos and Nonlinear Dynamics in Science and Engineering. Springer, Berlin (2013)
14. Dubois, M., Rubio, M., Berge, P.: Experimental evidence of intermittencies associated with a subharmonic bifurcation. Phys. Rev. Lett. **16**, 1446–1449 (1983)
15. Malasoma, J., Werny, P., Boiron, M.: Multichannel type I intermittency in two models of Rayleigh–Benard convection. Phys. Rev. Lett. **51**, 487–500 (2004)
16. Stavrinides, S., Miliou, A., Laopoulos, T., Anagnostopoulos, A.: The intermittency route to chaos of an electronic digital oscillator. Int. J. Bifurc. Chaos **18**, 1561–1566 (2008)
17. Sanmartin, J., Lopez-Rebollal, O., del Rio, E., Elaskar, S.: Hard transition to chaotic dynamics in Alfven wave-fronts. Phys. Plasmas **11**, 2026–2035 (2004)
18. Sanchez-Arriaga, G., Sanmartin, J., Elaskar, S.: Damping models in the truncated derivative nonlinear Schrödinger equation. Phys. Plasmas **14**, 082108 (2007)
19. Pizza, G., Frouzakis, C., Mantzaras, J.: Chaotic dynamics in premixed hydrogen/air channel flow combustion. Combust. Theor. Model. **16**, 275–299 (2012)
20. Nishiura, Y., Ueyama, D., Yanagita, T.: Chaotic pulses for discrete reaction diffusion systems. SIAM J. Appl. Dyn. Syst. **4**, 723–754 (2005)
21. de Anna, P., Le Borgne, T., Dentz, M., Tartakovsky, A., Bolster, D., Davy, P.: Flow intermittency, dispersion and correlated continuous time random walks in porous media. Phys. Rev. Lett. **110**, 184502 (2013)
22. Stan, C., Cristescu, C., Dimitriu, D.: Analysis of the intermittency behavior in a low-temperature discharge plasma by recurrence plot quantification. Phys. Plasmas **17**, 042115 (2010)
23. Chian, A.: Complex System Approach to Economic Dynamics. Lecture Notes in Economics and Mathematical Systems, pp. 39–50. Springer, Berlin (2007)
24. Zebrowski, J., Baranowski, R.: Type I intermittency in nonstationary systems: models and human heart-rate variability. Physica A **336**, 74–86 (2004)
25. Paradisi, P., Allegrini, P., Gemignani, A., Laurino, M., Menicucci, D., Piarulli, A.: Scaling and intermittency of brains events as a manifestation of consciousness. AIP Conf. Proc. **1510**, 151–161 (2012)

26. del Rio, E., Elaskar, S.: New characteristic relation in type II intermittency. Int. J. Bifurc. Chaos **20**, 1185–1191 (2010)
27. Elaskar, S., del Rio, E., Donoso, J.: Reinjection probability density in type III intermittency. Physica A **390**, 2759–2768 (2011)
28. del Rio, E., Sanjuan, M., Elaskar, S.: Effect of noise on the reinjection probability density in intermittency. Commun. Nonlinear Sci. Numer. Simul. **17**, 3587–3596 (2012)
29. Elaskar, S., del Rio, E.: Intermittency reinjection probability function with and without noise effects. In: Latest Trends in Circuits, Automatics Control and Signal Processing, pp. 145–154. ISBN: 978-1-61804-131-9, Barcelona (2012)
30. del Rio, E., Elaskar, S., Makarov, S.: Theory of intermittency applied to classical pathological cases. Chaos **23**, 033112 (2013)
31. del Rio, E., Elaskar, S., Donoso, J.: Laminar length and characteristic relation in type I intermittency. Commun. Nonlinear Sci. Numer. Simul. **19**, 967–976 (2014)
32. Krause, G., Elaskar, S., del Rio, E.: Type I intermittency with discontinuous reinjection probability density in a truncation model of the derivative nonlinear Schrödinger equation. Nonlinear Dyn. **77**, 455–466 (2014)
33. Krause, G., Elaskar, S., del Rio, E.: Noise effect on statistical properties of type I intermittency. Physica A **402**, 318–329 (2014)
34. Elaskar, S., del Río, E., Krause, G., Costa, A.: Effect of the lower boundary of reinjection and noise in type II intermittency. Nonlinear Dyn. **79**, 1411–1424 (2015)
35. del Río, E., Elaskar, S.: On the intermittency theory. Int. J. Bifurc. Chaos **26**, 1650228 (2016)
36. del Rio, E., Elaskar S.: The intermittency route to chaos. In: Skiadas, C.H., Skiadas, C. (eds.) Handbook of Applications of Chaos Theory, pp. 3–20. CRC Press Book. ISBN 9781466590434. Paris (2016)
37. Elaskar, S., del Río, E., Costa, A.: Reinjection probability density for type III intermittency with noise and lower boundary of reinjection. J. Comp. Nonlinear Dyn. **12**, 031020-11 (2017)
38. Bauer, M., Habip, S., He, D., Martiessen, W.: New type of intermittency in discontinuous maps. Phys. Rev. Lett. **68**, 1625–1628 (1992)
39. He, D., Bauer, M., Habip, S., Kruger, U., Martiessen, W., Christiansen, B., Wang, B.: Type V intermittency. Phys. Lett. A **171**, 61–65 (1992)
40. Fan, J., Ji, F., Guan, S., Wang, B., He, D.: The distribution of laminar lengths in type V intermittency. Phys. Lett. A **182**, 232–237 (1993)
41. Wu, S., He, D.: Characteristics of period-doubling bifurcation cascades in quasidiscontinuous systems. Commun. Theor. Phys. **35**, 275–282 (2001)
42. Wang, D., Mo, J., Zhao, X., Gu, H., Qu, S., Ren, W.: Intermittent chaotic neural firing characterized by non-smooth like features. Chin. Phys. Lett. **27**, 070503 (2010)
43. Gu, H., Xiao, W.: Difference between intermittent chaotic bursting and spiking of neural firing patterns. Int. J. Bifurc. Chaos **24**, 1450082 (2014)
44. Bai-lin, H.: Elementary Symbolic Dynamics and Chaos in Dissipative Systems. World Scientific, Singapore (1989)